

pubs.acs.org/JPCC Article

# Tuning between Methylammonium Lead Bromide Perovskite Magic-Sized Clusters and Quantum Dots through Ligand Assisted Reprecipitation at Elevated Temperatures

Published as part of The Journal of Physical Chemistry virtual special issue "Horst Weller Festschrift".

Melissa Guarino-Hotz, Jeremy L. Barnett, Liem B. Pham, Allison A. Win, Vivien L. Cherrette, and Jin Z. Zhang\*



Cite This: J. Phys. Chem. C 2022, 126, 13854–13862



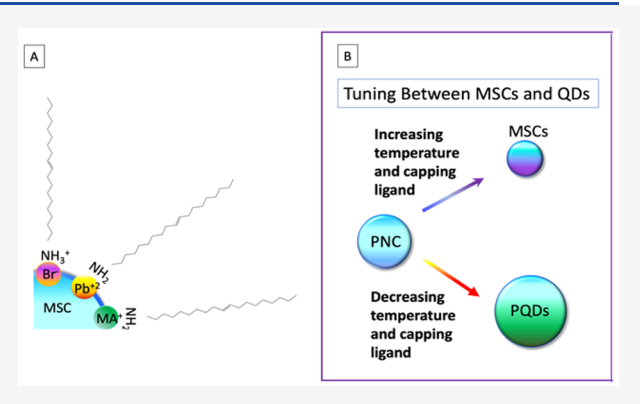
**ACCESS** 

Metrics & More

Article Recommendations

s) Supporting Information

ABSTRACT: Methylammonium lead bromide perovskite magic-sized clusters and quantum dots were synthesized using a new heated ligand assisted reprecipitation (HLARP) technique using organic amines and acids as capping ligands. The optical properties of these nanoparticles were analyzed using UV—vis electronic absorption and photoluminescent spectroscopy. Varying the temperature of the precursor solution while keeping the antisolvent temperature consistent allows for tuning between perovskite magic-sized clusters (MSCs) and quantum dots (PQDs) without the need to use excessive concentrations of capping ligand. Higher precursor solution temperatures favor MSCs, while lower temperatures favor PQDs. Furthermore, increasing the temperature of the system shifts the original emission band from 436 to 453 nm, by increasing the size and



potentially through the introduction of surface defects. Low frequency Raman spectroscopy reveals that MSCs have vibrational frequencies that are similar to those of bulk perovskite. Electrospray mass spectrometry and infrared spectroscopy were used to probe the ligands on the surface of the MSCs, indicating that amine is the primary capping ligand and the surface is presumably cation rich.

## **■ INTRODUCTION**

Perovskite quantum dots (PQDs) have been studied extensively for their unique properties, such as high photoluminescence (PL) quantum yield and tunable optical properties. Their emission can be easily tuned over the entire visible spectrum by controlling the crystal size,<sup>2,3</sup> capping ligand, 4,5 and elemental composition. 6,7 These distinctive optoelectronic properties make them promising substrates for applications in the fields of photovoltaics for light-emitting devices, <sup>8,9</sup> photodetectors, <sup>10,11</sup> and sensing. <sup>12,13</sup> The tunable emission of PQDs stems from their quantum confinement and high surface to volume (S/V) ratio. 14,15 By comparison, perovskite magic-sized clusters (MSCs) are smaller, more monodispersed and have narrower, bluer optical absorption bands.<sup>4,5,16-21</sup> They are often described as kinetic products or stable intermediaries of PQDs.<sup>22</sup> Understanding the relationship between PQDs and MSCs can aid in fundamental studies of the growth mechanism of quantum dots and bulk perovskite.

As MSCs have such a high S/V ratio, they are susceptible to surface dangling bonds and defect sites leading to instability. <sup>23,24</sup> Thus, MSCs are typically formed by increasing the

concentration of molecular capping ligands with appropriate anchoring functional groups to increase surface protection. To date, a significant amount of work has been dedicated to tuning between MSCs and PQDs by varying ligand composition and concentration. <sup>5,18,25,26</sup> These syntheses typically employ ligand-assisted reprecipitation (LARP) at room temperature. For instance, Xu et al. demonstrated that an increase in trivalent metal hydrated nitrate coordination complexes yields monodispersed MSCs. <sup>4</sup> Using a similar process, Li et al. demonstrated that increasing the concentration of organic acid and amine ligands also yields MSCs exclusively. Moreover, increasing the concentration of organic amine alone also favors the production of MSCs. <sup>5</sup> It was determined that amine was likely a strong capping ligand, which allowed it to more

Received: June 23, 2022 Revised: July 26, 2022 Published: August 4, 2022





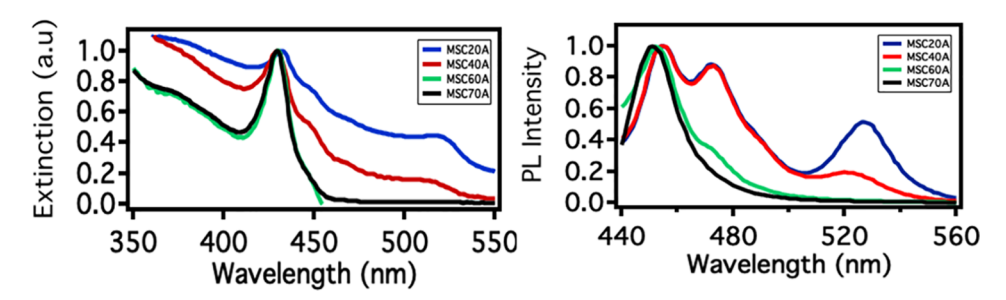


Figure 1. (left) Normalized UV-vis absorption and (right) normalized PL spectra of MAPbBr<sub>3</sub> PQDs and MSCs capped with 0.15 mmol of oleylamine and oleic acid with various precursor temperatures.

effectively passivate a smaller particle. However, nanocrystal formation is dependent on a multitude of variables. By varying the temperature, quantum dots have been synthesized using the hot injection method.<sup>27</sup> This requires high temperatures (120–140 °C) and is typically performed in an air-free environment, heating both precursor and antisolvent solutions, but typically results in an increase of monodispersity and particle stability.<sup>28,29</sup> However, for MSCs, other variables have barely been explored and little research has been done using temperature for tuning.<sup>30</sup> In the Gibbs—Thomson equation, the temperature and critical radius are inversely proportional.

Thus, increasing the temperature results in smaller nanoparticles by imparting more energy to the surface, allowing them to stabilize at smaller sizes.<sup>31</sup> However, in the synthesis presented herein, the solution is rapidly cooled from an elevated temperature to around 20 °C. Rapid cooling during a crystallization process decreases the size of crystal formation by increasing the number of collisions and speeding up the formation time scale.<sup>32</sup> Moreover, rapid cooling increases the number of nucleation sites, encouraging many particles to form at the same time and more rapidly depleting available resources, causing smaller particles to form. 33 However, rapid cooling can cause more defects in the crystal structure, as it forms the kinetic, not thermodynamic, product.<sup>34</sup> Defects can lead to modifications in the Stokes shift, where emission occurs at a longer wavelength than absorption does, 35 and defect engineering can be useful to tune the optical properties of nanoparticles for different applications like solar cells or photovoltaics.36

In this work, MSCs and PQDs are synthesized using a new heated ligand assisted reprecipitation (HLARP) technique using organic amines and acids as capping ligands. The optical properties of these nanoparticles were analyzed using UV—vis and photoluminescence spectroscopy. Higher precursor solution temperatures favor MSCs, while lower temperatures favor PQDs. Moreover, increasing the temperature of the system allows the formation of stable states of MSCs to be tuned from the original emission band of 436 to 453 nm. Low frequency Raman spectroscopy was used to gain structural insights. Electrospray mass spectrometry and infrared spectroscopy were used to determine that MSCs are primarily capped with amine, indicating that the surface of the MSCs is cation rich.

## METHODS

**Materials.** Methylammonium bromide (MABr, 99.9%, Greatcell Solar), PbBr<sub>2</sub> (99.999%, Alfa Aesar), valeric acid (99.0% Alfa Aesar), *n*-octanoic acid (98.0%, Tokyo Chemical Industry), oleic acid (90%, Sigma-Aldrich), *n*-octylamine (98.0%, Tokyo Chemical Industry), *N*,*N*-dimethylformamide

(DMF, 99.9%, Fisher Scientific), hydrobromic acid (HBr, 48%, Honeywell), and toluene (99.9%, Fisher Scientific) were commercially available. All chemicals were used as received without any further purification.

**Synthesis of MAPbBr**<sub>3</sub> **PQDs and MSCs.** In a modified LARP synthesis process of PQDs and MSCs, MABr (0.080 mmol, 9.0 mg), PbBr<sub>2</sub> (0.20 mmol, 73.0 mg), and 400  $\mu$ L of DMF were added to a borosilicate vial, and the solution was sonicated in a water bath between 20 and 70 °C until all solid dissolved. Next, organic acid (oleic, octyl, or valeric) of varying amounts (0.15, 0.30, and 1.0 mmol) was added to the solution and sonicated at this temperature for 30 s. Then, amine (oleyl or octyl) of equimolar amounts was added to the solution and sonicated for 30 s at temperature. One hundred microliters of the precursor solution was injected at a fast rate into 5.0 mL of toluene under vigorous stirring. Particles were washed through centrifugation, first at 5000 rpm, retaining the supernatant, and then twice at 10 000 rpm, keeping the pellet.

Control experiments were conducted by repeating this process without the addition of oleic acid, doubling the amount of oleic acid, or replacing oleic acid with an equimolar amount of hydrobromic acid.

**Spectroscopic Measurements.** Ultraviolet—visible (UV—vis) absorption spectra were measured with an Agilent Technologies Cary 60 UV—vis spectrophotometer, and the PL spectra were measured using a Cary Eclipse spectro-fluorometer using a quartz 700  $\mu$ L microcuvette at room temperature and an excitation wavelength of 400 nm. FTIR spectra were obtained with a PerkinElmer FTIR spectrometer (Spectrum One, a spectral resolution of 4 cm<sup>-1</sup>), where the samples were prepared by dropping the MAPbBr<sub>3</sub> nanoparticle solutions onto salt plates for analysis.

**Mass Spectrometry.** The washed particles with less than 10 mM concentration in 50% methanol were analyzed by direct sample injection from a syringe needle with a 10  $\mu$ L/min flow rate on a Thermo Electron Finnigan LTQ mass spectrometer in positive mode or negative mode over a full scan range of m/z 50–1000. The voltage was set to 5.0 kV with a capillary temperature of 275 °C. Data were analyzed by using the XCalibur software.

## ■ RESULTS AND DISCUSSION

Tuning Between PQDs and MSCs. MAPbBr<sub>3</sub> nanoparticles of varying sizes capped with 0.15 mmol of oleylamine and oleic acid were synthesized using a new HLARP method. The precursor solution was heated to 20, 40, 60, or 70 °C and injected into room temperature antisolvent. Nanoparticles formed at different precursor temperatures with 0.15 mmol of capping ligand were subsequently labeled as MSC20A—MSC70A. Their UV—vis absorption and PL spectra are

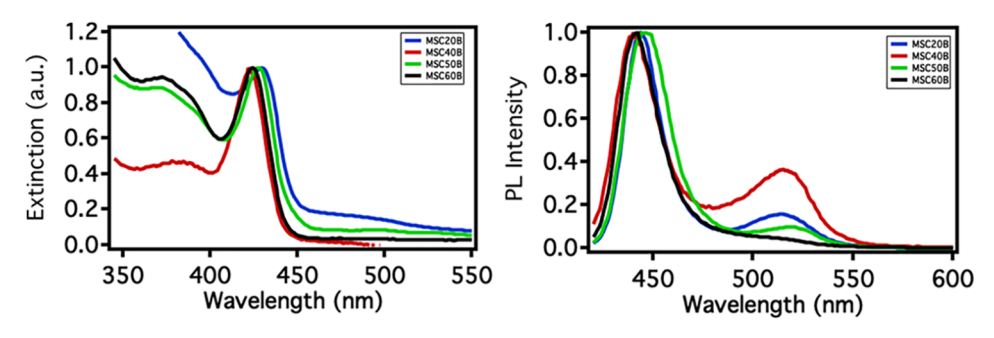


Figure 2. (left) Normalized UV-vis absorption and (right) normalized PL spectra of MAPbBr<sub>3</sub> PQDs and MSCs capped with 0.30 mmol of oleylamine and oleic acid with various precursor temperatures.

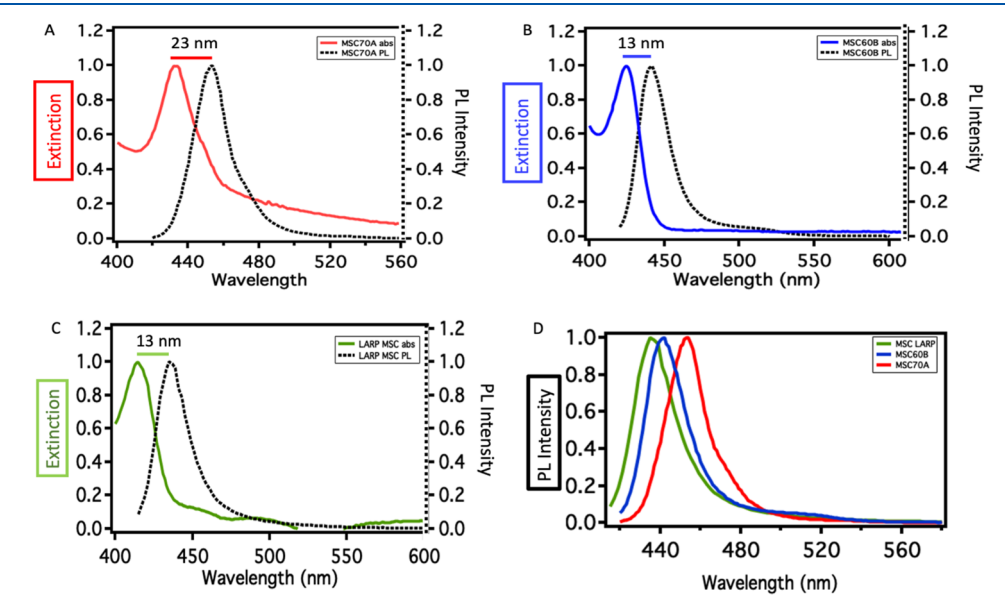


Figure 3. Combined normalized UV-vis and PL data for (A) MSC70A, (B) MSC60B, and (C) MAPbBr<sub>3</sub> oleylamine and oleic acid synthesized using the original LARP method. (D) Normalized PL spectra of MSC70A, MSC60B, and LARP MSCs compared directly.

shown in Figure 1. Three absorption bands are observed for MSC20A and MSC40A at 430, 450, and 519 nm. In the case of MSC60A and MSC70A, there is only one absorption band at 430 nm. According to previous studies, the range of 450–520 nm broader excitonic absorption peaks is attributed to PQDs. 5,37,38 while the single sharp excitonic absorption peak at around 430 nm is assigned to MSCs. 5,25,26,39

In the PL spectra, three emission peaks at 455, 473, and 528 nm were observed for MSC20A and MSC40A. Two emission peaks were observed for MSC60A at 450 and 473 nm. Finally, only one emission peak at 453 nm was observed for MSC70A. The fwhm is 19 nm, indicating a narrow distribution of sizes. The PL emission peak at 528 and 473 nm corresponds to PQDs of differing sizes, while the strong and sharp excitonic emission peak at 450 nm is assigned to MSCs. It should be noted that MSCs synthesized with the HLARP method use 15% less capping ligand than that used in previously reported LARP methods.<sup>5</sup> HLARP MSCs formed with less capping ligand with rapid cooling exhibited a Stokes shift of 23 nm, compared to previous reports with a 6 nm shift produced with the LARP method with excess octylamine and octanoic acid at room temperature.<sup>5</sup> Details of the UV-vis absorption and PL emission peaks of MAPbBr<sub>3</sub> PQDs and MSCs with various ligands at differing temperatures are summarized in the Supporting Information.

This synthesis is predicated on the principles that increasing the temperature increases the surface free energy necessary to decrease the critical radius<sup>31,40</sup> of a nanoparticle and that rapid cooling causes crystal formation to occur on a faster time scale. 41-43 Thus, increasing the temperature of the precursor solution increases this free energy, allowing for the formation of smaller particles. Moreover, increasing the temperature increases the solubility of the capping ligands, allowing for better nanoparticle/capping ligand interaction and leading to more effective passivation, which helps with stabilization at a smaller size.<sup>44</sup> Additionally, by injecting heated precursor into a room temperature antisolvent, the solution supersaturates due to two factors, both solvent and temperature changes.<sup>45</sup> Thus, the equilibrium is shifted toward crystallization on a shorter time scale than those synthesized using the LARP method. Rapid cooling also facilitates the production of more nucleation sites, which decreases the concentration of precursors, inhibits Ostwald ripening, and thus forms smaller particles.<sup>33</sup> Since MSCs synthesized using HLARP form more rapidly, they are not the most thermodynamically stable product but a stable intermediary.

The HLARP synthesis of MAPbBr<sub>3</sub> PQDs and MSCs was repeated using double the amount of oleic acid and oleylamine, 0.30 mmol, at a lower temperature range of 20–60 °C. Figure 2 shows UV–vis absorption and PL spectra with a similar trend. Here there are fewer absorption bands compared to 0.15

mmol of capping ligand as shown in Figure 1. MSC20B-60B produces one major absorption band around 427 nm. The intensity of the shoulder from 470 to 510 nm, indicating PQDs, diminishes with the increase in temperature of the precursor solution. As expected, the increase in capping ligand increases the production of MSCs. However, it also arrested the production of the 450 nm absorbing particles. The growth of MSCs is typically described as discrete, where there is a thermodynamic barrier to the growth of a larger size. He is possible that the addition of excess capping ligand is preventing collisions that provide energy to overcome this barrier and form a larger crystal.

In the PL spectra, there is one broad emission peak at 515 nm, attributed to PQDs, and one sharp peak ranging from 440 to 446 nm associated with MSCs. As the temperature increased, the 515 nm peak disappeared and the 446 nm peak blue-shifted to 440 nm. MSC60B showed one narrow peak at 440 nm with a fwhm of 22 nm, indicating a monodispersed population of particles. Increasing the capping ligand concentration of the synthesis blue-shifted the MSCs, which likely indicates a reduction in particle radius. Here monodispersity is achieved at a lower temperature, thus indicating that there is not a universal transition point to overcome the activation energy to form MSCs. However, their Stokes shift is 13 nm and thus still larger than those in many reported LARP methods<sup>4,5,17</sup> but smaller than the 23 nm shift of MSC70A.

**Tunability of MSCs.** The monodispersed MSCs from Figures 1 and 2 are compared directly in Figure 3 to the original LARP synthesis and show the tunability of the MSCs emission band. A characteristic feature of MSCs is their discrete, monodispersed size. S,45 There is a 17 nm difference in the emission position between the MSC70A and the MSCs from the original LARP method (Figure 3D), which emit at 453 and 436 nm, respectively. The Stokes shift also increases from 13 to 23 nm using the HLARP synthesis. The MSC60B emission peak is red-shifted by 4 nm from the original LARP MSCs, but both have a Stokes shift of 13 nm.

The optical properties of these nanoparticles are governed by quantum confinement, <sup>14</sup> and thus, changing their size will affect their band gap. A size-dependent band gap can be made with the Brus method, <sup>38,39,47</sup>

$$E_g(MSCs) = E_g(bulk) + \frac{h^2}{8r^2} \left( \frac{1}{m_e} + \frac{1}{m_h} \right)$$
 (1)

where  $E_{\rm g}({\rm MSCs})$  is the band gap of MSCs,  $E_{\rm g}$  is the band gap of bulk perovskite, h is Planck's constant, r is the radius,  $m_{\rm e}$  is the mass of the electron, and  $m_{\rm h}$  is the mass of the hole. From previous reports,  $E_{\rm g}$  (bulk) was previously determined to be 2.30 eV<sup>48</sup> and  $\left(\frac{1}{m_{\rm e}} + \frac{1}{m_{\rm h}}\right)$  was determined to be 2.37  $\times$  10<sup>30</sup> kg<sup>-1</sup>.<sup>21</sup>

The sizes of MSCs LARP, MSC60B, and MSC70A were calculated to be 3.05, 3.13, and 3.41 nm, respectively. As MSCs have such a high S/V ratio, they are particularly vulnerable to trap states formed through surface defects. By synthesizing MSCs with less capping ligand, a higher temperature is required to form monodispersed MSCs. Increasing the temperature also introduces rapid cooling, which has been shown to introduce more defects into the nanoparticle. The defects may affect radiative recombination and result in the larger Stokes shift. By contrast, using a larger concentration

of capping ligand, a lower temperature was needed to synthesize MSCs with a more blue-shifted emission for MSC60B. The MSCs surface defects were more effectively passivated, and crystal formation could occur on a slightly larger time scale. As these crystals are likely more "perfect", they have less defects to create trap states. Thus, radiative recombination occurs without as much electron—phonon coupling. This would agree with the previously reported MSCs synthesized with excess capping ligand forming at room temperature. They are likely to have a decrease in defects or trap states, resulting in a smaller Stokes shift. This tunability allows them to be optimized for different applications. A larger Stokes shift is desirable for solar cell applications to minimize photon reabsorption, 51,52 while a smaller Stokes shift is more applicable for photovoltaics to achieve a higher power conversion efficiency. 52,53

**Structural Properties.** Figure 4 shows the low frequency Raman of the MSCs in solution. The MSC vibrational modes

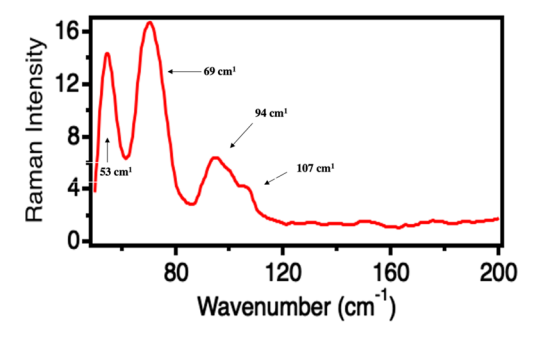


Figure 4. Low frequency Raman spectrum of  $MAPbBr_3$  MSCs in solution measured with a 785 nm laser.

were compared to those of methylammonium lead bromide bulk. The characteristic mode at 53 cm<sup>-1</sup> indicates octahedra distortion<sup>54</sup> and the bending of lead halide bonds.<sup>55</sup> The modes at 69 and 94 cm<sup>-1</sup> are due to lurching methylammonium, <sup>54</sup> and the mode at 107 cm<sup>-1</sup> is due to methylammonium libations.<sup>55</sup> Comparing to theoretical spectra of MAPbBr<sub>3</sub> in its tetrahedral-1, tetrahedral-2, and orthorhombic phases, the 94 cm<sup>-1</sup> is well accounted for in the tetrahedral-2 formation and in the octahedral formation, not in the tetrahedral-1 formation. All four modes of the nanocrystal are in good agreement with bulk methylammonium lead bromide.<sup>54</sup> This is somewhat unexpected since, given their small size, one might expect higher vibrational frequencies than those for bulk. Future theoretical studies may help to provide some explanation or new insight into this.

**Surface Ligand Binding.** Figure 5 compares the IR spectra of oleic acid, oleylamine, and MSCs emitting at 453 nm. Oleylamine shows characteristic modes of oleyl groups. The peaks at 2851-2853 and 2922-2925 cm<sup>-1</sup> are due to the symmetric and asymmetric CH<sub>2</sub> stretching modes, respectively, and peaks at 3003-3006 cm<sup>-1</sup> are assigned to the  $\nu$ (C–H) mode of the C–H bond adjacent to the C=C bond. It also shows C–H bending modes at 1468 cm<sup>-1</sup>. The spectrum is distinguished by the sharpness of the modes at 2922-2925 cm<sup>-1</sup> and 2851-2853 cm<sup>-1</sup>. S6

Oleic acid similarly shows the characteristic modes of oleyl groups at 2851-2853, 2922-2925, 3003-3006, and 1468 cm<sup>-1</sup>. However, it has characteristic modes of the carboxylic acid group. The  $\nu(C=O)$  mode is observed as a sharp, strong peak at 1707 cm<sup>-1</sup>, an additional C-H bending mode at 1450

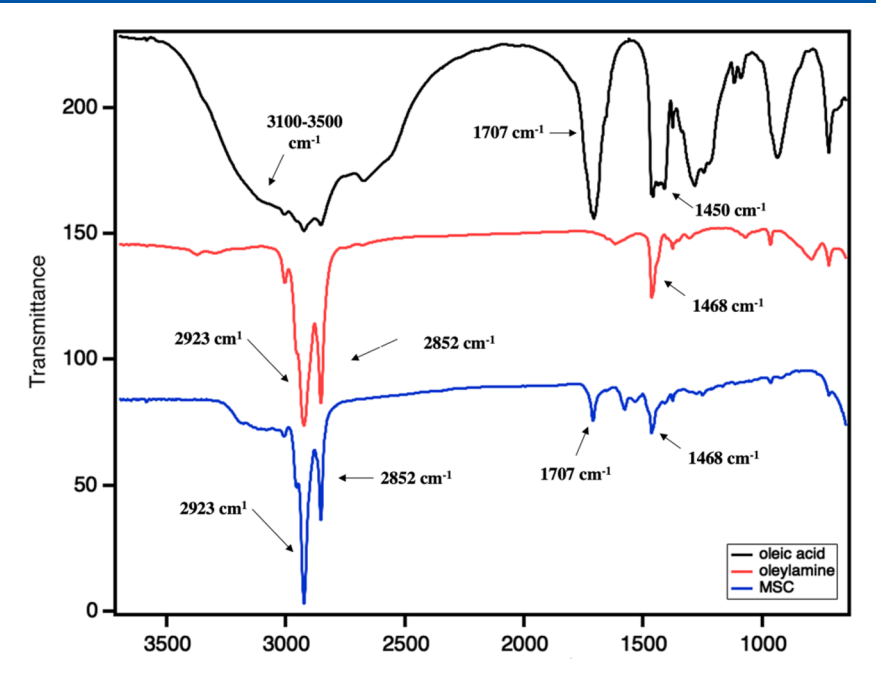
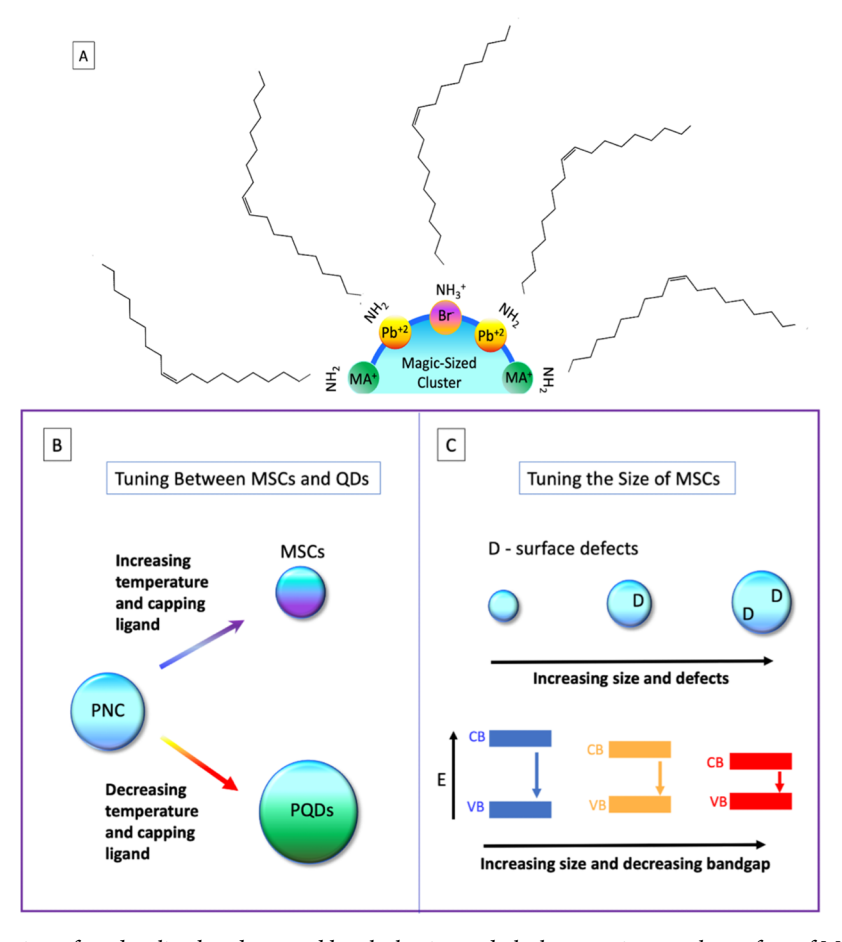


Figure 5. IR spectra of oleylamine (red), oleic acid (black), and MSCs (blue).



**Figure 6.** (A) Potential cationic surface dangling bonds capped by oleylamine and oleyl ammonium on the surface of MSCs. (B) Description of the growth mechanism to tune between MSCs and PQDs using temperature, capping ligand concentration, and rapid cooling. (C) Comparison of size of MSCs, defects, and band gap of a PNC-perovskite nanocrystal.

cm<sup>-1</sup>, and a broad shoulder in the region between 3100 and 3500 cm<sup>-1</sup>, which could be assigned to dimers of oleic acid in a bilayer structure. <sup>56</sup>

The FTIR spectrum of MSCs shows all the oleyl group modes. It also shows a peak at 1707 cm<sup>-1</sup> that can be attributed to the carbonyl group of oleic acid. The low

intensity of the peak indicates a low concentration. The spectrum also shows the characteristic sharp peaks at 2923 and 2852 cm<sup>-1</sup>, characteristic of oleylamine, suggesting both amine and acid ligands are present on the surface.<sup>57</sup> Moreover, a combination of the protonated and deprotonated form of each capping ligand is likely to interact due to a proton transfer reaction between the two. However, the protonated and deprotonated forms of these compounds are difficult to distinguish using IR. Moreover, IR spectroscopy alone is insufficient to quantify the molar ratio of ligands on the surface; thus, mass spectrometry was employed to gain insight.<sup>56</sup>

Figure S3 shows the positive ion mass spectrum of MSCs emitting at 453 nm. Washed particles were injected directly into an ESI mass spectrometer and positive and negative ion spectra were obtained. The positive ion spectrum shows a characteristic peak at 268 m/z, indicating ionized oleylamine or oleyl ammonium (Figure S3). As equimolar amounts of oleylamine and oleic acid were used in the synthesis of these MSCs, an oleic acid or oleate peak would be expected. However, the requisite 281 m/z peak is not present (Figure S4). This is intriguing as common passivation theories of metal halide perovskites accept the cocktail approach, using many types of capping ligands to passivate different defects.<sup>24</sup> While oleic acid is still present on the surface, as shown by the IR spectrum, oleylamine or oleyl ammonium is the predominant capping ligand. To confirm these findings, MSCs were synthesized with exclusively oleylamine and oleyl ammonium as capping ligands (Figure S4). Oleylamine alone could effectively result in the generation of MSCs. Two control experiments were conducted using oleyl ammonium, which was generated from oleylamine using an excess of oleic acid and with an equimolar amount of hydrobromic acid. The acidified mixtures yielded a mixture of MSCs and PQDs. Thus, acidification of oleylamine does not yield monodispersed MSCs. Since oleylamine by itself does yield MSCs, it is likely the primary capping ligand.

These results are consistent with Liu et al.'s findings that increased oleylamine yields more MSCs. However, here we confirm that oleylamine is the primary capping ligand bound on the surface of the MSCs. Since capping ligands are used to passivate surface defects, we can infer a significant amount about the surface chemistry based on which capping ligand is on the surface. The FTIR spectra confirm the presence of oleylamine and a small amount of oleic acid. The presence of oleic acid is shown in the FTIR spectra, but nothing about its binding to the surface is known. As oleylamine and oleic acid interact via an acid-base neutralization to form oleyl ammonium and oleate,5 we likely have oleyl ammonium and oleate present on the surface as well. As is consistent with the literature, the combination of these ligands will effectively passivate several anionic and cationic defects more effectively than one ligand alone.<sup>24</sup> However, with such a large, confirmed presence of oleylamine present on the surface, the MSC surface is likely cation rich as oleylamine acts as an electron donator.49

As shown in Figure 6A, we propose that the surface of MSCs is primarily capped with oleylamine and a small amount of oleyl ammonium. Different defects are usually anticipated for perovskite nanocrystals, such as MSCs and PQDs, in relation to different components, MA<sup>+</sup>, Pb<sup>2+</sup>, or Br<sup>-.49</sup> When both oleylamine and oleic acid are used as ligands, they react to form oleyl ammonium and oleate. Thus, oleylamine, oleyl

ammonium, oleate, and oleic acid are all expected to play some role in passivating or binding to the cationic and anion defects on the surface on the nanocrystal, as observed in PQDs.<sup>24</sup> It is expected that these ligands passivate with similar molar amounts, as observed in the mass spectrum of CsPbI<sub>3</sub> PQDs.<sup>58</sup> However, Liu et al. showed that MSC formation occurs with an increase in amine concentration, and the mass spectrum presented herein, along with control experiments (Figure S5), shows that MSCs are predominantly capped using oleylamine in its deprotonated form. Amines donate a lone pair of electrons that datively coordinates positively charged surface atoms.<sup>59</sup> Thus, the surface seems cation rich, with likely methylammonium and lead defects dominating over halide anions. There are likely a small percentage of Br defects on the surface that are passivated by oleyl ammonium. Li et al. proposed that amines could act as a stronger capping ligand<sup>5</sup> and long chain primary amines provide excellent surface coverage, leading to more effective passivation and smaller particle size. 60 This suggests a correlation between smaller particles and cationic surface environments.

Figure 6B illustrates the tuning effects of temperature and capping ligand concentration on MSCs and PQDs. In this work, we see the equilibrium shift to MSCs from PQDs by increasing the capping ligand concentration and the temperature of the precursor solution. Using an excessive amount of capping ligand usually leads to better passivation and reduced particle size.<sup>4,5</sup> Capping ligands help lower the surface free energy and stabilize particles at a smaller critical radius. 33,42,43 Meanwhile, increasing the temperature helps to overcome the energy barriers for formation and results in the stabilization of smaller particles. 33,42,43 It also facilitates the formation of nucleation sites and increases the solubility of capping ligands, both of which favor smaller particles.<sup>61</sup> Moreover, the nanocrystals also undergo rapid cooling during formation, which inhibits Ostwald ripening, similarly lowering the critical radius.<sup>33</sup> Both of these variables used in conjunction allow not only for the tuning between MSCs and PQDs but also for varying the size of MSCs.

As quantum size confinement affects both MSCs and PQDs, tuning their size has significant implications on their band gaps (Figure 6C). 62 While the tunability of PQDs has been well established, 1,63-71 the tunability of MSCs is less explored since they are often described as discrete. 45,72 In this work, MSCs show a tunable emission from 436 to 453 nm. This emission band shift may also be due to a change in band edge defect states (Figure 6C). In addition to the size difference, there is also an increase in the magnitude of the Stokes shift when switching from smaller particles, like MSC LARP and MSC60B, to larger particles, like MSC70A.<sup>35</sup> MSC70A was formed using a 50 °C temperature differential from rapid cooling. Rapid cooling results in smaller particles and causes crystal formation to occur on a shorter time scale. This can also lead to more defects often responsible for trap state emission.<sup>34</sup> Thus, the kinetic barrier is overcome, but there is no time to reach thermodynamic equilibrium. By increasing the temperature in conjunction with increasing capping ligand concentration, MSCs exhibit tunable emission bands through both potential defect introduction and size variability.

## CONCLUSIONS

Methylammonium lead bromide magic-sized clusters and quantum dots are synthesized using a new heated ligand assisted reprecipitation technique using organic amines and acids as capping ligands. UV-vis and PL spectroscopy were used to confirm the changes between PQDs and MSCs by varying the temperature of the precursor solution while keeping the antisolvent temperature consistent, without the need to use an excessive concentration of capping ligand. It was found that higher precursor solution temperatures favor MSCs while lower temperatures favor PQDs. Moreover, increasing the temperature of the system allows the emission band of MSCs to be tuned from 436 to 453 nm along with an increased Stokes shift from 13 to 23 nm potentially through the introduction of surface defects. Low frequency Raman results agree with that of bulk MAPbBr3, suggesting that the core of the MSCs has a very similar crystal or unit cell structure as that of bulk, which is interesting because, given their small size, one may expect higher vibrational frequencies than those for bulk. Since the HLARP synthesis utilizes less capping ligand, IR spectroscopy and mass spectrometry could be used to determine that amine was the primary capping ligand bound on the surface of the MSCs. This indicates that the surface of the MSCs is cation rich.

#### ASSOCIATED CONTENT

## Supporting Information

The Supporting Information is available free of charge at https://pubs.acs.org/doi/10.1021/acs.jpcc.2c04384.

Additional experimental details and supplemental data including UV—vis and PL data for PQDs and MSCs synthesized with 0.15 mmol of octylamine and octanoic acid; UV—vis and PL data for PQDs and MSCs synthesized with 0.15 mmol of octylamine and valeric acid; positive scan mode mass spectrum of MSCs capped with oleylamine and oleic acid; negative scan mode mass spectrum of MSCs capped with oleylamine and oleic acid; zoomed in negative scan mode mass spectrum of MSCs capped with oleylamine and oleic acid; and UV—vis and PL spectra of MSCs capped only oleylamine, excess oleic acid and oleylamine, and oleylamine with HBr (PDF)

## AUTHOR INFORMATION

#### **Corresponding Author**

Jin Z. Zhang — Department of Chemistry and Biochemistry, University of California, Santa Cruz, California 95064, United States; o orcid.org/0000-0003-3437-912X; Email: zhang@ucsc.edu

## **Authors**

Melissa Guarino-Hotz — Department of Chemistry and Biochemistry, University of California, Santa Cruz, California 95064, United States; occid.org/0000-0001-6310-8156

Jeremy L. Barnett – Department of Chemistry and Biochemistry, University of California, Santa Cruz, California 95064, United States

Liem B. Pham – Department of Chemistry and Biochemistry, University of California, Santa Cruz, California 95064, United States

Allison A. Win – Department of Chemistry and Biochemistry, University of California, Santa Cruz, California 95064, United States Vivien L. Cherrette – Department of Chemistry and Biochemistry, University of California, Santa Cruz, California 95064, United States

Complete contact information is available at: https://pubs.acs.org/10.1021/acs.jpcc.2c04384

#### **Author Contributions**

The manuscript was written through contributions of all authors. All authors have given approval to the final version of the manuscript.

#### **Notes**

The authors declare no competing financial interest.

### ACKNOWLEDGMENTS

We are grateful to NSF (CHE-1904547) and NASA (MACES, Grant NNX15AQ01A) for financial support.

#### REFERENCES

- (1) Wang, H.-C.; Bao, Z.; Tsai, H.-Y.; Tang, A.-C.; Liu, R.-S. Perovskite Quantum Dots and Their Application in Light-Emitting Diodes. *Small* **2018**, *14* (1), 1702433.
- (2) Chen, X.; Peng, L.; Huang, K.; Shi, Z.; Xie, R.; Yang, W. Non-Injection Gram-Scale Synthesis of Cesium Lead Halide Perovskite Quantum Dots with Controllable Size and Composition. *Nano Research* **2016**, 9 (7), 1994–2006.
- (3) Leng, J.; Wang, T.; Zhao, X.; Ong, E. W. Y.; Zhu, B.; Ng, J. D. A.; Wong, Y.-C.; Khoo, K. H.; Tamada, K.; Tan, Z.-K. Thermodynamic Control in the Synthesis of Quantum-Confined Blue-Emitting CsPbBr3 Perovskite Nanostrips. *J. Phys. Chem. Lett.* **2020**, *11* (6), 2036–2043.
- (4) Xu, K.; Allen, A. C.; Luo, B.; Vickers, E. T.; Wang, Q.; Hollingsworth, W. R.; Ayzner, A. L.; Li, X.; Zhang, J. Z. Tuning from Quantum Dots to Magic Sized Clusters of CsPbBr3 Using Novel Planar Ligands Based on the Trivalent Nitrate Coordination Complex. J. Phys. Chem. Lett. 2019, 10 (15), 4409–4416.
- (5) Liu, L.; Xu, K.; Vickers, E. T.; Allen, A. C.; Li, X.; Peng, L.; Zhang, J. Varying the Concentration of Organic Acid and Amine Ligands Allows Tuning between Quantum Dots and Magic-Sized Clusters of CH3NH3PbBr3 Perovskite: Implications for Photonics and Energy Conversion. ACS Appl. Nano Mater. 2020, 3, 12379.
- (6) Lou, Y.; Fang, M.; Chen, J.; Zhao, Y. Formation of Highly Luminescent Cesium Bismuth Halide Perovskite Quantum Dots Tuned by Anion Exchange. *Chem. Commun.* **2018**, *54* (30), 3779–3782.
- (7) Wang, H.; Sui, N.; Bai, X.; Zhang, Y.; Rice, Q.; Seo, F. J.; Zhang, Q.; Colvin, V. L.; Yu, W. W. Emission Recovery and Stability Enhancement of Inorganic Perovskite Quantum Dots. *J. Phys. Chem. Lett.* **2018**, 9 (15), 4166–4173.
- (8) Wei, Y.; Cheng, Z.; Lin, J. An Overview on Enhancing the Stability of Lead Halide Perovskite Quantum Dots and Their Applications in Phosphor-Converted LEDs. *Chem. Soc. Rev.* **2019**, 48 (1), 310–350.
- (9) Wang, S.; Wang, Y.; Zhang, Y.; Zhang, X.; Shen, X.; Zhuang, X.; Lu, P.; Yu, W. W.; Kershaw, S. V.; Rogach, A. L. Cesium Lead Chloride/Bromide Perovskite Quantum Dots with Strong Blue Emission Realized via a Nitrate-Induced Selective Surface Defect Elimination Process. *J. Phys. Chem. Lett.* **2019**, *10* (1), 90–96.
- (10) Bi, C.; Kershaw, S. V.; Rogach, A. L.; Tian, J. Improved Stability and Photodetector Performance of CsPbI3 Perovskite Quantum Dots by Ligand Exchange with Aminoethanethiol. *Adv. Funct. Mater.* **2019**, 29 (29), 1902446.
- (11) Zhang, Z.-X.; Li, C.; Lu, Y.; Tong, X.-W.; Liang, F.-X.; Zhao, X.-Y.; Wu, D.; Xie, C.; Luo, L.-B. Sensitive Deep Ultraviolet Photodetector and Image Sensor Composed of Inorganic Lead-Free Cs3Cu2I5 Perovskite with Wide Bandgap. *J. Phys. Chem. Lett.* **2019**, 10 (18), 5343–5350.

- (12) Lu, L.-Q.; Tan, T.; Tian, X.-K.; Li, Y.; Deng, P. Visual and Sensitive Fluorescent Sensing for Ultratrace Mercury Ions by Perovskite Quantum Dots. *Anal. Chim. Acta* **2017**, 986, 109–114.
- (13) Wang, Y.; Zhu, Y.; Huang, J.; Cai, J.; Zhu, J.; Yang, X.; Shen, J.; Jiang, H.; Li, C. CsPbBr3 Perovskite Quantum Dots-Based Monolithic Electrospun Fiber Membrane as an Ultrastable and Ultrasensitive Fluorescent Sensor in Aqueous Medium. *J. Phys. Chem. Lett.* **2016**, 7 (21), 4253–4258.
- (14) Dong, Y.; Qiao, T.; Kim, D.; Parobek, D.; Rossi, D.; Son, D. H. Precise Control of Quantum Confinement in Cesium Lead Halide Perovskite Quantum Dots via Thermodynamic Equilibrium. *Nano Lett.* **2018**, *18* (6), 3716–3722.
- (15) Tyagi, P.; Arveson, S. M.; Tisdale, W. A. Colloidal Organohalide Perovskite Nanoplatelets Exhibiting Quantum Confinement. *J. Phys. Chem. Lett.* **2015**, *6* (10), 1911–1916.
- (16) Stein, J. L.; Steimle, M. I.; Terban, M. W.; Petrone, A.; Billinge, S. J. L.; Li, X.; Cossairt, B. M. Cation Exchange Induced Transformation of InP Magic-Sized Clusters. *Chem. Mater.* **2017**, 29 (18), 7984–7992.
- (17) Xu, K.; Vickers, E. T.; Luo, B.; Allen, A. C.; Chen, E.; Roseman, G.; Wang, Q.; Kliger, D. S.; Millhauser, G. L.; Yang, W.; et al. First Synthesis of Mn-Doped Cesium Lead Bromide Perovskite Magic Sized Clusters at Room Temperature. *J. Phys. Chem. Lett.* **2020**, *11* (3), 1162–1169.
- (18) Liu, L.; Pan, K.; Xu, K.; Zhang, J. Z. Impact of Molecular Ligands in the Synthesis and Transformation between Metal Halide Perovskite Quantum Dots and Magic Sized Clusters. *ACS Phys. Chem. Au* **2022**, 2 (3), 156–170.
- (19) Vickers, E. T.; Chen, Z.; Cherrette, V.; Smart, T.; Zhang, P.; Ping, Y.; Zhang, J. Z. Interplay between Perovskite Magic-Sized Clusters and Amino Lead Halide Molecular Clusters. *Research* (*Washington, DC, U. S.*) **2021**, *7*, 6047971.
- (20) White, S. L.; Banerjee, P.; Chakraborty, I.; Jain, P. K. Ion Exchange Transformation of Magic-Sized Clusters. *Chem. Mater.* **2016**, 28, 8391.
- (21) Vickers, E. T.; Xu, K.; Dreskin, B. W.; Graham, T. A.; Li, X.; Zhang, J. Z. Ligand Dependent Growth and Optical Properties of Hybrid Organo-Metal Halide Perovskite Magic Sized Clusters. *J. Phys. Chem. C* 2019, 123 (30), 18746–18752.
- (22) Jiang, Z.-J.; Kelley, D. F. Role of Magic-Sized Clusters in the Synthesis of CdSe Nanorods. ACS Nano 2010, 4 (3), 1561–1572.
- (23) Nevers, D. R.; Williamson, C. B.; Hanrath, T.; Robinson, R. D. Surface Chemistry of Cadmium Sulfide Magic-Sized Clusters: A Window into Ligand-Nanoparticle Interactions. *Chem. Commun.* **2017**, *53* (19), 2866–2869.
- (24) Zhang, J. Z. A "Cocktail" Approach to Effective Surface Passivation of Multiple Surface Defects of Metal Halide Perovskites Using a Combination of Ligands. *J. Phys. Chem. Lett.* **2019**, *10* (17), 5055–5063.
- (25) Xu, K.; Allen, A. C.; Luo, B.; Vickers, E. T.; Wang, Q.; Hollingsworth, W. R.; Ayzner, A. L.; Li, X.; Zhang, J. Z. Tuning from Quantum Dots to Magic Sized Clusters of CsPbBr3 Using Novel Planar Ligands Based on the Trivalent Nitrate Coordination Complex. J. Phys. Chem. Lett. 2019, 10 (15), 4409–4416.
- (26) Xu, K.; Vickers, E. T.; Luo, B.; Wang, Q.; Allen, A. C.; Wang, H.; Cherrette, V.; Li, X.; Zhang, J. Z. Room Temperature Synthesis of Cesium Lead Bromide Perovskite Magic Sized Clusters with Controlled Ratio of Carboxylic Acid and Benzylamine Capping Ligands. Sol. Energy Mater. Sol. Cells 2020, 208, No. 110341.
- (27) Zhang, L. J.; Shen, X.-C.; Liang, H.; Yao, J. T. Multiple Families of Magic-Sized ZnSe Quantum Dots via Noninjection One-Pot and Hot-Injection Synthesis. *J. Phys. Chem. C* **2010**, *114* (50), 21921–21927.
- (28) de Mello Donega, C.; Liljeroth, P.; Vanmaekelbergh, D. Physicochemical Evaluation of the Hot-Injection Method, a Synthesis Route for Monodisperse Nanocrystals. *Small* **2005**, *1* (12), 1152–1162.
- (29) Kamat, P. V. Quantum Dot Solar Cells. The Next Big Thing in Photovoltaics. *J. Phys. Chem. Lett.* **2013**, *4* (6), 908–918.

- (30) Permatasari, F. A.; Masitoh, H. E.; Mahen, E. C. S.; Nuryadin, B. W.; Aimon, A. H.; Syah, Y. M.; Iskandar, F. Synergetic Effect of the Surface Ligand and SiO2 Driven Photoluminescence Stabilization of the CH3NH3PbBr3 Perovskite Magic-Sized Clusters. *Sci. Rep* **2021**, *11* (1), 22211.
- (31) Pu, Y.-C.; Song, F.; Zhang, W.; Lindley, S.; Adams, S.; Zhang, J. Z. Size-Tunable Synthesis of Hollow Gold Nanospheres through Control of Reaction Temperature. *Particle & Particle Systems Characterization* **2017**, 34 (8), 1600255.
- (32) Stein, S. Cooling Rate and Crystal Size. https://sites.northwestern.edu/sethstein/a-small-is-beautiful-approach-to-upgrading-a-beginning-geophysics-course/cooling-rate-and-crystal-size/ (accessed 2022-03-23).
- (33) Madras, G.; McCoy, B. J. Temperature Effects on the Transition from Nucleation and Growth to Ostwald Ripening. *Chem. Eng. Sci.* **2004**, *59* (13), 2753–2765.
- (34) Zhou, Y.; Sun, X.; Zhong, K.; Evans, D. G.; Lin, Y.; Duan, X. Control of Surface Defects and Agglomeration Mechanism of Layered Double Hydroxide Nanoparticles. *Ind. Eng. Chem. Res.* **2012**, *51* (11), 4215–4221.
- (35) Tan, A. M. Z.; Garcia, M. A.; Hennig, R. G. Giant Stokes Shift for Charged Vacancies in Monolayer SnS. *Phys. Rev. Materials* **2022**, *6* (4), No. 044003.
- (36) Xu, S.; Zhong, G.; Chen, C.; Zhou, M.; Kline, D. J.; Jacob, R. J.; Xie, H.; He, S.; Huang, Z.; et al. Uniform, Scalable, High-Temperature Microwave Shock for Nanoparticle Synthesis through Defect Engineering. *Matter* **2019**, *1* (3), 759–769.
- (37) Vickers, E. T.; Enlow, E. E.; Delmas, W. G.; DiBenedetto, A. C.; Chowdhury, A. H.; Bahrami, B.; Dreskin, B. W.; Graham, T. A.; Hernandez, I. N.; Carter, S. A.; et al. Enhancing Charge Carrier Delocalization in Perovskite Quantum Dot Solids with Energetically Aligned Conjugated Capping Ligands. *ACS Energy Lett.* **2020**, 5 (3), 817–825.
- (38) Xu, K.; Vickers, E. T.; Rao, L.; Lindley, S. A.; Allen, A. C.; Luo, B.; Li, X.; Zhang, J. Z. Synergistic Surface Passivation of CH3NH3PbBr3 Perovskite Quantum Dots with Phosphonic Acid and (3-Aminopropyl)Triethoxysilane. *Chem. Eur. J.* **2019**, 25 (19), 5014–5021.
- (39) Vickers, E. T.; Xu, K.; Dreskin, B. W.; Graham, T. A.; Li, X.; Zhang, J. Z. Ligand Dependent Growth and Optical Properties of Hybrid Organo-Metal Halide Perovskite Magic Sized Clusters. *J. Phys. Chem. C* 2019, 123 (30), 18746–18752.
- (40) Thanh, N. T. K.; Maclean, N.; Mahiddine, S. Mechanisms of Nucleation and Growth of Nanoparticles in Solution. *Chem. Rev.* **2014**, *114* (15), 7610–7630.
- (41) Stefanescu, D. M. Equilibrium and Non-Equilibrium during Solidification. In *Science and Engineering of Casting Solidification*, Second ed.; Springer US: Boston, 2009; pp 1–20. DOI: 10.1007/978-0-387-74612-8 2.
- (42) Shen, Y.; Chen, R.; Yu, X.; Wang, Q.; Jungjohann, K. L.; Dayeh, S. A.; Wu, T. Gibbs—Thomson Effect in Planar Nanowires: Orientation and Doping Modulated Growth. *Nano Lett.* **2016**, *16* (7), 4158–4165.
- (43) Scalfi, L.; Coasne, B.; Rotenberg, B. On the Gibbs—Thomson Equation for the Crystallization of Confined Fluids. *J. Chem. Phys.* **2021**, *154* (11), 114711.
- (44) Silva, F. O.; Carvalho, M. S.; Mendonça, R.; Macedo, W. A.; Balzuweit, K.; Reiss, P.; Schiavon, M. A. Effect of Surface Ligands on the Optical Properties of Aqueous Soluble CdTe Quantum Dots. *Nanoscale Res. Lett.* **2012**, *7* (1), 536.
- (45) Pun, A. B.; Mazzotti, S.; Mule, A. S.; Norris, D. J. Understanding Discrete Growth in Semiconductor Nanocrystals: Nanoplatelets and Magic-Sized Clusters. *Acc. Chem. Res.* **2021**, *54* (7), 1545–1554.
- (46) Pun, A. B.; Mazzotti, S.; Mule, A. S.; Norris, D. J. Understanding Discrete Growth in Semiconductor Nanocrystals: Nanoplatelets and Magic-Sized Clusters. *Acc. Chem. Res.* **2021**, *54* (7), 1545–1554.

- (47) Bawendi, M. G.; Steigerwald, M. L.; Brus, L. E. The Quantum Mechanics of Larger Semiconductor Clusters ("Quantum Dots"). Annu. Rev. Phys. Chem. 1990, 41 (1), 477-496.
- (48) Harrell, S. M.; McBride, J. R.; Rosenthal, S. J. Synthesis of Ultrasmall and Magic-Sized CdSe Nanocrystals. Chem. Mater. 2013, 25 (8), 1199-1210.
- (49) Smart, T. J.; Takenaka, H.; Pham, T. A.; Tan, L. Z.; Zhang, J. Z.; Ogitsu, T.; Ping, Y. Enhancing Defect Tolerance with Ligands at the Surface of Lead Halide Perovskites. J. Phys. Chem. Lett. 2021, 12 (27), 6299-6304.
- (50) Wheeler, D. A.; Zhang, J. Z. Exciton Dynamics in Semiconductor Nanocrystals. Adv. Mater. 2013, 25 (21), 2878-2896.
- (51) Meinardi, F.; Colombo, A.; Velizhanin, K. A.; Simonutti, R.; Lorenzon, M.; Beverina, L.; Viswanatha, R.; Klimov, V. I.; Brovelli, S. Large-Area Luminescent Solar Concentrators Based on 'Stokes-Shift-Engineered' Nanocrystals in a Mass-Polymerized PMMA Matrix. Nature Photon 2014, 8 (5), 392-399.
- (52) Liu, Y.; Kim, D.; Morris, O. P.; Zhitomirsky, D.; Grossman, J. C. Origins of the Stokes Shift in PbS Quantum Dots: Impact of Polydispersity, Ligands, and Defects. ACS Nano 2018, 12 (3), 2838-
- (53) Ushakova, E. V.; Litvin, A. P.; Parfenov, P. S.; Fedorov, A. V.; Artemyev, M.; Prudnikau, A. V.; Rukhlenko, I. D.; Baranov, A. V. Anomalous Size-Dependent Decay of Low-Energy Luminescence from PbS Quantum Dots in Colloidal Solution. ACS Nano 2012, 6 (10), 8913-8921.
- (54) Leguy, A. M. A.; Goñi, A. R.; Frost, J. M.; Skelton, J.; Brivio, F.; Rodríguez-Martínez, X.; Weber, O. J.; Pallipurath, A.; Alonso, M. I.; Campoy-Quiles, M.; et al. Dynamic Disorder, Phonon Lifetimes, and the Assignment of Modes to the Vibrational Spectra of Methylammonium Lead Halide Perovskites. Phys. Chem. Chem. Phys. 2016, 18 (39), 27051–27066.
- (55) Quarti, C.; Grancini, G.; Mosconi, E.; Bruno, P.; Ball, J. M.; Lee, M. M.; Snaith, H. J.; Petrozza, A.; De Angelis, F. The Raman Spectrum of the CH3NH3PbI3 Hybrid Perovskite: Interplay of Theory and Experiment. J. Phys. Chem. Lett. 2014, 5 (2), 279-284.
- (56) Perez De Berti, I.; Cagnoli, M.; Pecchi, G.; Alessandrini, J.; Stewart, S.; Bengoa, F.; Marchetti, S. Alternative Low-Cost Approach to the Synthesis of Magnetic Iron Oxide Nanoparticles by Thermal Decomposition of Organic Precursors. Nanotechnology 2013, 24, No. 175601.
- (57) Salavati-Niasari, M.; Fereshteh, Z.; Davar, F. Synthesis of Oleylamine Capped Copper Nanocrystals via Thermal Reduction of a New Precursor. Polyhedron 2009, 28 (1), 126-130.
- (58) Kim, J.; Cho, S.; Dinic, F.; Choi, J.; Choi, C.; Jeong, S. M.; Lee, J.-S.; Voznyy, O.; Ko, M. J.; Kim, Y. Hydrophobic Stabilizer-Anchored Fully Inorganic Perovskite Quantum Dots Enhance Moisture Resistance and Photovoltaic Performance. Nano Energy 2020, 75, No. 104985.
- (59) Boles, M. A.; Ling, D.; Hyeon, T.; Talapin, D. V. The Surface Science of Nanocrystals. Nat. Mater. 2016, 15 (2), 141–153.
- (60) Green, M. The Nature of Quantum Dot Capping Ligands. J. Mater. Chem. 2010, 20 (28), 5797-5809.
- (61) Zhang, L.-J.; Shen, X.-C.; Liang, H.; Yao, J.T. Multiple Families of Magic-Sized ZnSe Quantum Dots via Noninjection One-Pot and Hot-Injection Synthesis. J. Phys. Chem. C 2010, 114 (50), 21921-
- (62) Elward, J. M.; Chakraborty, A. Effect of Dot Size on Exciton Binding Energy and Electron-Hole Recombination Probability in CdSe Quantum Dots. J. Chem. Theory Comput. 2013, 9 (10), 4351-
- (63) Song, W.-S.; Yang, H. Efficient White-Light-Emitting Diodes Fabricated from Highly Fluorescent Copper Indium Sulfide Core/ Shell Quantum Dots. Chem. Mater. 2012, 24 (10), 1961-1967.
- (64) Song, W.-S.; Yang, H. Fabrication of White Light-Emitting Diodes Based on Solvothermally Synthesized Copper Indium Sulfide Quantum Dots as Color Converters. Appl. Phys. Lett. 2012, 100 (18), 183104.

- (65) Pietryga, J. M.; Park, Y.-S.; Lim, J.; Fidler, A. F.; Bae, W. K.; Brovelli, S.; Klimov, V. I. Spectroscopic and Device Aspects of Nanocrystal Quantum Dots. Chem. Rev. 2016, 116 (18), 10513-10622.
- (66) Zhang, R.; Yang, P.; Wang, Y. Facile Synthesis of CuInS2/ZnS Quantum Dots with Highly near-Infrared Photoluminescence via Phosphor-Free Process. J. Nanopart. Res. 2013, 15 (9), 1910.
- (67) Moreels, I.; Justo, Y.; De Geyter, B.; Haustraete, K.; Martins, J. C.; Hens, Z. Size-Tunable, Bright, and Stable PbS Quantum Dots: A Surface Chemistry Study. ACS Nano 2011, 5 (3), 2004-2012.
- (68) Song, W. S.; Yang, H. Efficient White-Light-Emitting Diodes Fabricated from Highly Fluorescent Copper Indium Sulfide Core/ Shell Quantum Dots. Chem. Mater. 2012, 24 (10), 1961-1967.
- (69) Protesescu, L.; Yakunin, S.; Bodnarchuk, M. I.; Krieg, F.; Caputo, R.; Hendon, C. H.; Yang, R. X.; Walsh, A.; Kovalenko, M. V. Nanocrystals of Cesium Lead Halide Perovskites (CsPbX 3, X = Cl, Br, and I): Novel Optoelectronic Materials Showing Bright Emission with Wide Color Gamut. Nano Lett. 2015, 15 (6), 3692-3696.
- (70) Liu, X.; Jiang, Y.; Lan, X.; Li, S.; Wu, D.; Han, T.; Zhong, H.; Zhang, Z. Synthesis of High Quality and Stability CdS Quantum Dots with Overlapped Nucleation-Growth Process in Large Scale. J. Colloid Interface Sci. 2011, 354 (1), 15-22.
- (71) Stein, J. L.; Mader, E. A.; Cossairt, B. M. Luminescent InP Quantum Dots with Tunable Emission by Post-Synthetic Modification with Lewis Acids. J. Phys. Chem. Lett. 2016, 7 (7), 1315-1320.
- (72) Mule, A. S.; Mazzotti, S.; Rossinelli, A. A.; Aellen, M.; Prins, P. T.; van der Bok, J. C.; Solari, S. F.; Glauser, Y. M.; Kumar, P. V.; Riedinger, A.; et al. Unraveling the Growth Mechanism of Magic-Sized Semiconductor Nanocrystals. J. Am. Chem. Soc. 2021, 143 (4), 2037-2048.

## **□** Recommended by ACS

## Localized Co<sup>2+</sup> Doping of CdSe/CdS Seeded Nanorods

Danja Fischli, Klaus Boldt, et al.

JULY 14, 2022

THE JOURNAL OF PHYSICAL CHEMISTRY C

READ **Z** 

## Large Stokes Shifts over Visible-Infrared Wavelengths from Multicore/Shell Quantum Dots for Solar-Harvesting **Applications**

Chang-Wei Yeh, Hsueh-Shih Chen, et al.

FEBRUARY 25, 2022

ACS APPLIED NANO MATERIALS

READ **C** 

## Near-Infrared-Emitting Cd, Hg, Se-Based Core/Shell **Nanoplatelets**

Andrei Mitrofanov, Alexander Eychmüller, et al.

SEPTEMBER 21, 2021

CHEMISTRY OF MATERIALS

READ **C** 

## Ligand-Induced Nucleation Growth Kinetics of CdTe QDs: Implications for White-Light-Emitting Diodes

Yanqing Luo, Chengyu Li, et al.

JANUARY 04, 2022

ACS APPLIED NANO MATERIALS

READ 2

Get More Suggestions >